

QUADRATIC AND CUBIC LAGRANGE FINITE ELEMENTS FOR MIXED LAPLACE EIGENVALUE PROBLEMS ON CRISS-CROSS MESHES

KAIBO HU, JIGUANG SUN, AND QIAN ZHANG

ABSTRACT. In [6], it was shown that the linear Lagrange element space on criss-cross meshes and its divergence exhibit spurious eigenvalues when applied in the mixed formulation of the Laplace eigenvalue problem, despite satisfying both the inf-sup condition and ellipticity on the discrete kernel. The lack of a Fortin interpolation is responsible for the spurious eigenvalues produced by the linear Lagrange space. In contrast, results in [8] confirm that quartic and higher-order Lagrange elements do not yield spurious eigenvalues on general meshes without nearly singular vertices, including criss-cross meshes as a special case. In this paper, we investigate quadratic and cubic Lagrange elements on criss-cross meshes. We prove the convergence of discrete eigenvalues by fitting the Lagrange elements on criss-cross meshes into a complex and constructing a Fortin interpolation. As a by-product, we construct bounded commuting projections for the finite element Stokes complex, which induces isomorphisms between cohomologies of the continuous and discrete complexes. We provide numerical examples to validate the theoretical results.

1. INTRODUCTION

Let $\Omega \subset \mathbb{R}^2$ be a simply-connected Lipschitz polygonal domain. The Laplace eigenvalue problem is to seek $u \in H_0^1(\Omega)$ such that

$$-\Delta u = \lambda u \text{ in } \Omega. \quad (1.1)$$

Introducing $\sigma = \text{grad } u$, we can obtain the mixed formulation: find (σ, u, λ) in $H(\text{div}; \Omega) \times L^2(\Omega) \times \mathbb{R}$ such that

$$\begin{aligned} (\sigma, \tau) + (u, \text{div } \tau) &= 0 & \forall \tau \in H(\text{div}; \Omega), \\ (\text{div } \sigma, v) &= -\lambda(u, v) & \forall v \in L^2(\Omega). \end{aligned} \quad (1.2)$$

Given finite dimensional subspaces V_h and W_h of $H(\text{div}; \Omega)$ and $L^2(\Omega)$, respectively, the mixed finite element approximation reads: find $(\sigma_h, u_h, \lambda_h)$ in $V_h \times W_h \times \mathbb{R}$ such that

$$\begin{aligned} (\sigma_h, \tau_h) + (u_h, \text{div } \tau_h) &= 0 & \forall \tau_h \in V_h, \\ (\text{div } \sigma_h, v_h) &= -\lambda_h(u_h, v_h) & \forall v_h \in W_h. \end{aligned} \quad (1.3)$$

It is shown in [6] that inappropriate choices of finite element pair V_h and W_h would lead to spurious eigenvalues. To ensure the convergence of the finite element approximation (1.3) to (1.2), it is crucial that the spaces V_h and W_h satisfy the inf-sup condition, ellipticity on the discrete kernel, as well as an additional condition related to the Fortin interpolation. The

Key words and phrases. Lagrange finite element, Fortin interpolation, mixed Laplace eigenvalue problem, bounded commuting projections.

Nédélec finite element space of order k for V_h and the piecewise polynomial space of order $k - 1$ for W_h satisfy these conditions, and can therefore produce correctly convergent eigenvalues [5, 7].

In contrast to the Nédélec finite elements, the Lagrange finite element space of order k for V_h and its divergence for W_h produce correctly convergent eigenvalues only on spacial triangulations. In [8], Boffi et al. rigorously proved the convergence of such a pair $V_h - W_h$ for the Maxwell eigenvalue problem on the Powell-Sabin triangulation when $k = 1$, Clough-Tocher triangulation when $k = 2$, and general shape-regular triangulations without nearly singular vertices when $k \geq 4$. They achieve this by constructing Fortin-type interpolations. As Problem (1.2) is equivalent to the mixed form of the Maxwell eigenvalue problem considered in [8] by rotating σ by $-\pi/2$, the results in [8] indicate that the quartic and higher-order Lagrange finite element spaces lead to correctly convergent finite element schemes for Problem (1.2) on criss-cross meshes. Whereas, as shown in [6], the linear Lagrange element space on the criss-cross mesh exhibits spurious eigenvalues due to the lack of a Fortin interpolation. To the best of our knowledge, there have been no previous studies investigating the behavior of quadratic and cubic Lagrange elements on criss-cross meshes for problem (1.2). This paper aims to fill this gap.

In this paper, we establish the convergence of discrete eigenvalues computed from (1.3) with quadratic and cubic Lagrange elements on criss-cross meshes for V_h . Our analysis relies on the existence of bounded Fortin operators. To construct the Fortin interpolation, we fit the quadratic and cubic Lagrange element spaces V_h on the criss-cross mesh into a subcomplex of the Stokes complex, as shown in the following diagram,

$$\begin{array}{ccccccccc}
 0 & \longrightarrow & \mathbb{R} & \xrightarrow{\subset} & H^2(\Omega) & \xrightarrow{\text{curl}} & \mathbf{H}^1(\Omega) & \xrightarrow{\text{div}} & L^2(\Omega) & \longrightarrow & 0 \\
 & & & & \downarrow & & \downarrow & & \downarrow & & \\
 0 & \longrightarrow & \mathbb{R} & \xrightarrow{\subset} & \Sigma_h & \xrightarrow{\text{curl}} & V_h & \xrightarrow{\text{div}} & \text{div } V_h & \longrightarrow & 0.
 \end{array} \tag{1.4}$$

The H^2 -conforming finite element space Σ_h on the criss-cross mesh is available in the literature [11] and $V_h\text{-div } V_h$ is shown to be inf-sup stable for the Stokes problem [3]. Nevertheless, to the best of our knowledge, the sequence (1.4), which links these spaces, has not been presented yet. Using the finite element subcomplex (1.4), we can redefine the degrees of freedom (DOFs) for V_h . The canonical interpolation defined by the new DOFs satisfies the necessary commutativity, but it cannot serve as a Fortin interpolation for Problem (1.3) since the boundedness requires more smoothness. We will use the Scott-Zhang interpolation to fix this boundedness issue. We note that our approach differs from [8], where a Fortin-type interpolation is constructed for functions that have piecewise-polynomial divergence. To use the mixed formulation (1.3), we also provide a characterization of the space $\text{div } V_h$. Moreover, the cohomology of finite element spaces plays a crucial role in numerical computation for many problems (see, e.g., [1, 2, 4, 13]). Our Fortin interpolation, together with a Scott-Zhang type interpolation, leads to bounded commuting projections for complex (1.4), which induces isomorphisms between the cohomologies of (1.4).

The pair $V_h - \text{div } V_h$ in the diagram can also be used for solving the Stokes problem. In [3], Arnold and Qin use the quadratic Lagrange element space V_h for the Stokes problem. They used a piecewise polynomial space for pressure, which includes a spurious pressure mode. Consequently, a post-processing procedure is necessary to remove the spurious pressure mode from the numerical pressure. With the explicit characterization of $\text{div } V_h$ in our work, we can use the

pair $V_h - \operatorname{div} V_h$ to solve the Stokes problem, and the numerical pressure will converge without the need for post-processing.

The remaining part of the paper is organized as follows. In Section 2, we present notation, the discrete eigenvalue problem and an equivalent formulation, the source problem and solution operators, and a general theoretical framework. In Section 3, we present the definition of each space in the finite element Stokes complex, characterize the space $\operatorname{div} V_h$, and prove the cohomology of the complex. In Section 4, we construct a Fortin interpolation that satisfies desired properties. In Section 5, we construct bounded commuting projections for (1.4) and show their approximation property. In Section 6, we provide numerical examples to validate our convergence analysis.

2. SETTING OF THE PROBLEM

2.1. Notation. Let \mathcal{Q}_h be a partition of Ω with convex quadrilaterals. Each $Q \in \mathcal{Q}_h$ is further split into four triangles by the two diagonals of Q . We denote the triangulation of Q as \mathcal{T}_h^Q . Let \mathcal{T}_h be the partition of Ω with triangles in $\cup_{Q \in \mathcal{Q}_h} \mathcal{T}_h^Q$. We denote by h_T the diameter of an element $T \in \mathcal{T}_h$. Define $h = \max_{T \in \mathcal{T}_h} h_T$ to be the mesh size of \mathcal{T}_h . We define \mathcal{V}_h to be the set of vertices in the mesh \mathcal{Q}_h . For $Q \in \mathcal{Q}_h$, we denote by $\mathcal{V}_h(Q)$ and $\mathcal{E}_h(Q)$ the sets of vertices and edges of Q . Denote by \mathbf{n}_Q the unit outward normal vector to Q . For an edge e of $T \in \mathcal{T}_h$, we denote by \mathbf{n}_e the unit normal vector to e . For $Q \in \mathcal{Q}_h$, we define $h_Q = \max_{T \in \mathcal{T}_h^Q} h_T$.

We suppose the triangles in \mathcal{T}_h are shape-regular, i.e.,

$$\frac{h_T}{\rho_T} \leq \sigma_0,$$

where ρ_T is the radius of the largest closed ball contained in \bar{T} .

For any $Q \in \mathcal{Q}_h$, we can map $\hat{Q} = (-1, 1) \times (-1, 1)$ to Q by

$$\mathbf{x} = F_Q(\hat{\mathbf{x}}),$$

where $F_Q = F_i$ on T_i with $F_i(\hat{\mathbf{x}}) = B_i \hat{\mathbf{x}} + \mathbf{b}_i$ mapping \hat{T}_i to T_i , $i = 1, 2, 3, 4$. See Figure 2.1 for \hat{T}_i and T_i .

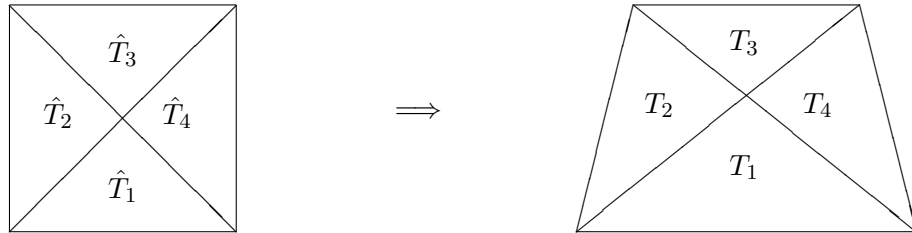


FIGURE 2.1. \hat{Q} (left) and Q (right)

For a simply-connected sub-domain $D \subset \Omega$, we adopt standard notation for Sobolev spaces such as $H^m(D)$ equipped with the norm $\|\cdot\|_{m,D}$ and the semi-norm $|\cdot|_{m,D}$. If $m = 0$, the space

$H^0(D)$ coincides with $L^2(D)$ equipped with the norm $\|\cdot\|_D$, and when $D = \Omega$, we drop the subscript D . We use $\mathbf{H}^m(D)$ and $\mathbf{L}^2(D)$ to denote the vector-valued Sobolev spaces $[H^m(D)]^2$ and $[L^2(D)]^2$.

We define

$$H(\operatorname{div}; \Omega) := \{\mathbf{u} \in \mathbf{L}^2(\Omega) : \operatorname{div} \mathbf{u} \in L^2(\Omega)\},$$

with the scalar products and norms $(\mathbf{u}, \mathbf{v})_{H(\operatorname{div}; \Omega)} = (\mathbf{u}, \mathbf{v}) + (\operatorname{div} \mathbf{u}, \operatorname{div} \mathbf{v})$ and $\|\mathbf{u}\|_{H(\operatorname{div}; \Omega)} = \sqrt{(\mathbf{u}, \mathbf{u})_{H(\operatorname{div}; \Omega)}}$.

We use $P_k(D)$ to denote the space of polynomials on D with degree of no larger than k and $\mathbf{P}_k(D) = [P_k(D)]^2$. We denote $\tilde{P}_k(D)$ as the space of homogeneous polynomials of order k .

2.2. Discrete Eigenvalue Problem. We use a supscript k to denote the polynomial degree of the space V_h ,

$$V_h^k = \{\mathbf{u} \in \mathbf{H}^1(\Omega) : \mathbf{u}|_T \in \mathbf{P}_k(T) \text{ for any } T \in \mathcal{T}_h\},$$

and let

$$W_h^{k-1} = \operatorname{div} V_h^k.$$

The finite element scheme is to find $(\boldsymbol{\sigma}_h, u_h, \lambda_h)$ in $V_h^k \times W_h^{k-1} \times \mathbb{R}$ such that

$$\begin{aligned} (\boldsymbol{\sigma}_h, \boldsymbol{\tau}_h) + (u_h, \operatorname{div} \boldsymbol{\tau}_h) &= 0 & \forall \boldsymbol{\tau}_h \in V_h^k, \\ (\operatorname{div} \boldsymbol{\sigma}_h, v_h) &= -\lambda_h(u_h, v_h) & \forall v_h \in W_h^{k-1}. \end{aligned} \quad (2.1)$$

In addition to the primal formulation which is to find $(u, \lambda) \in H^1(\Omega) \times \mathbb{R}$ such that

$$(\operatorname{grad} u, \operatorname{grad} v) = \lambda(u, v) \quad \forall u \in H^1(\Omega), \quad (2.2)$$

by taking $v = \operatorname{div} \boldsymbol{\tau}$ in (1.2), we can get another equivalent formulation: find $(\boldsymbol{\sigma}, \lambda)$ in $H(\operatorname{div}; \Omega) \times \mathbb{R}$ such that

$$(\operatorname{div} \boldsymbol{\sigma}, \operatorname{div} \boldsymbol{\tau}) = \lambda(\boldsymbol{\sigma}, \boldsymbol{\tau}) \quad \forall \boldsymbol{\tau} \in H(\operatorname{div}; \Omega). \quad (2.3)$$

An equivalent scheme is to find $(\boldsymbol{\sigma}_h, \lambda_h)$ in $V_h^k \times \mathbb{R}$ such that

$$(\operatorname{div} \boldsymbol{\sigma}_h, \operatorname{div} \boldsymbol{\tau}_h) = \lambda_h(\boldsymbol{\sigma}_h, \boldsymbol{\tau}_h) \quad \forall \boldsymbol{\tau}_h \in V_h^k. \quad (2.4)$$

With this formulation, we can compute the numerical eigenvalues without characterizing W_h^{k-1} .

2.3. Source Problem. We will need the corresponding source problem for the analysis. We define the solution operators $\mathbf{A} : L^2(\Omega) \rightarrow H(\operatorname{div}; \Omega)$ and $T : L^2(\Omega) \rightarrow L^2(\Omega)$ such that for a given $f \in L^2(\Omega)$, there holds

$$\begin{aligned} (\mathbf{A}f, \boldsymbol{\tau}) + (Tf, \operatorname{div} \boldsymbol{\tau}) &= 0 \quad \forall \boldsymbol{\tau} \in H(\operatorname{div}; \Omega), \\ (\operatorname{div} \mathbf{A}f, v) &= -(f, v) \quad \forall v \in L^2(\Omega). \end{aligned} \quad (2.5)$$

Similarly, we define the discrete solution operators $\mathbf{A}_h : L^2(\Omega) \rightarrow V_h^k$ and $T_h : L^2(\Omega) \rightarrow W_h^{k-1}$ such that for a given $f \in L^2(\Omega)$, there holds

$$\begin{aligned} (\mathbf{A}_h f, \boldsymbol{\tau}) + (T_h f, \operatorname{div} \boldsymbol{\tau}) &= 0 \quad \forall \boldsymbol{\tau} \in V_h^k, \\ (\operatorname{div} \mathbf{A}_h f, v) &= -(f, v) \quad \forall v \in W_h^{k-1}. \end{aligned} \quad (2.6)$$

Lemma 2.1. For $f \in L^2(\Omega)$, there exists a $\delta \in (0, 1/2]$ depending on the interior angles of Ω such that $\mathbf{A}f \in \mathbf{H}^{1/2+\delta}(\Omega)$ and $Tf \in H^{3/2+\delta}(\Omega)$. Moreover,

$$\begin{aligned}\|\mathbf{A}f\|_{1/2+\delta} &\leq C\|f\|, \\ \|Tf\|_{3/2+\delta} &\leq C\|f\|.\end{aligned}$$

Proof. From (2.5), we can obtain $\mathbf{A}f = \text{grad } Tf$ and $-\text{div } \mathbf{A}f = f$, which implies $-\Delta Tf = f$. Moreover, from the first equation of (2.5), we can get $Tf = 0$ on $\partial\Omega$. By the regularity estimate of the Laplace problem [12], we have $Tf \in H^{3/2+\delta}(\Omega)$ and $\|Tf\|_{3/2+\delta} \leq C\|f\|$. Then $\mathbf{A}f = \text{grad } Tf \in \mathbf{H}^{1/2+\delta}(\Omega)$ and $\|\mathbf{A}f\|_{1/2+\delta} \leq \|Tf\|_{3/2+\delta} \leq C\|f\|$. ■

From Lemma 2.1, we can see that

$$\mathbf{A}(L^2(\Omega)) = \mathbf{H}^{1/2+\delta}(\Omega) \cap H(\text{div}; \Omega), \quad T(L^2(\Omega)) = H^{3/2+\delta}(\Omega).$$

2.4. Theoretical Framework. Define

$$V = \mathbf{H}^{1/2+\delta}(\Omega) \cap H(\text{div}; \Omega),$$

and equip it with norm

$$\|\cdot\|_V = \left(\|\cdot\|_{1/2+\delta}^2 + \|\cdot\|_{H(\text{div}; \Omega)}^2 \right)^{1/2}.$$

Assumption 2.1. We assume that

H1. There exists a constant α such that

$$(\boldsymbol{\sigma}_h, \boldsymbol{\sigma}_h) \geq \alpha \|\boldsymbol{\sigma}_h\|_{H(\text{div}; \Omega)}^2 \text{ on } \mathbb{K}_h,$$

where $\mathbb{K}_h = \{\boldsymbol{\tau}_h \in V_h^k : (\text{div } \boldsymbol{\tau}_h, v_h) = 0 \text{ for any } v_h \in W_h^{k-1}\}$.

H2. There exists an L^2 -orthogonal projection $P_h : L^2(\Omega) \rightarrow W_h^{k-1}$ satisfying

$$\|\phi - P_h\phi\| \leq \omega_0(h) \|\text{grad } \phi\| \quad \forall \phi \in H^1(\Omega). \quad (2.7)$$

H3. There exists a Fortin interpolation $\Pi_h : V \rightarrow V_h^k$ such that for any $\boldsymbol{\tau} \in V$,

$$\text{div } \Pi_h \boldsymbol{\tau} = P_h \text{div } \boldsymbol{\tau}, \quad (2.8)$$

$$\|\boldsymbol{\tau} - \Pi_h \boldsymbol{\tau}\| \leq \omega_1(h) \|\boldsymbol{\tau}\|_V. \quad (2.9)$$

Here $\omega_i(h) > 0$ and $\lim_{h \rightarrow 0^+} \omega_i(h) = 0, i = 0, 1$.

According to [7, Theorem 3.2], under Assumption 2.1,

$$\|T - T_h\| \rightarrow 0,$$

which implies the convergence of the discrete eigenvalues computed from (2.1) and (2.4). Assumptions **H1** and **H2** are easy to verify. To construct a Fortin interpolation that satisfies **H3**, in the following section, we fit V_h^k and W_h^{k-1} into a finite element complex.

3. A FINITE ELEMENT DE RHAM COMPLEX ON \mathcal{Q}_h

For $k = 2, 3$, we will fit finite element spaces V_h^k and W_h^{k-1} into a finite element Stokes complexes:

$$0 \longrightarrow \mathbb{R} \xrightarrow{\subset} \Sigma_h^{k+1} \xrightarrow{\text{curl}} V_h^k \xrightarrow{\text{div}} W_h^{k-1} \longrightarrow 0. \quad (3.1)$$

To this end, we first construct local function spaces $\Sigma_h^{k+1}(Q)$, $V_h^k(Q)$, and $W_h^{k-1}(Q)$ such that they form a local de Rham complex:

$$0 \longrightarrow \mathbb{R} \xrightarrow{\subset} \Sigma_h^{k+1}(Q) \xrightarrow{\text{curl}} V_h^k(Q) \xrightarrow{\text{div}} W_h^{k-1}(Q) \longrightarrow 0, \quad (3.2)$$

where

$$\Sigma_h^{k+1}(Q) = \{u \in H^2(Q) : u|_T \in P_{k+1}(T) \text{ for any } T \in \mathcal{T}_h^Q\},$$

$$V_h^k(Q) = \{u \in H^1(Q) : u|_T \in P_k(T) \text{ for any } T \in \mathcal{T}_h^Q\}, \text{ and}$$

$$W_h^{k-1}(Q) = \text{div } V_h^k(Q).$$

We will present the DOFs for each space in the following paragraphs. The DOFs for each space are also shown in Figures 3.1 and 3.2.

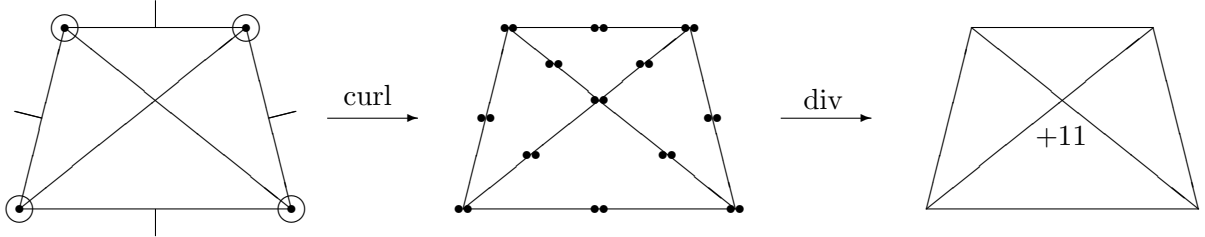


FIGURE 3.1. The finite element complex (3.2) with $k = 2$.

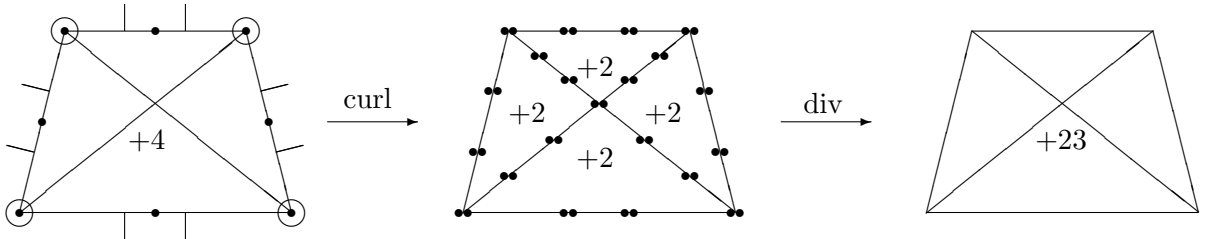


FIGURE 3.2. The finite element complex (3.2) with $k = 3$.

Space $\Sigma_h^{k+1}(Q)$. A function $u \in \Sigma_h^{k+1}(Q)$ can be determined by

- $u(v)$, $\partial_x u(v)$, $\partial_y u(v)$ for all $v \in \mathcal{V}_h(Q)$;
- $\int_e \partial_{n_e} u q ds$ for all $q = \hat{q} \circ F_Q^{-1}$ with $\hat{q} \in P_{k-2}(\hat{e})$ and $e \in \mathcal{E}_h(Q)$;
- $\frac{1}{|e|} \int_e u q ds$ for all $q = \hat{q} \circ F_Q^{-1}$ with $\hat{q} \in P_{k-3}(\hat{e})$ and $e \in \mathcal{E}_h(Q)$;
- $\frac{1}{|T|} \int_T u q dA$ for all $q = \hat{q} \circ F_Q^{-1}$ with $\hat{q} \in P_{k-4}(\hat{T})$ and $T \in \mathcal{T}_h^Q$.

Lemma 3.1. The above DOFs for space $\Sigma_h^{k+1}(Q)$ is unisolvent and H^2 -conforming.

Proof. The unisolvence and H^2 -conformity of $\Sigma_h^3(Q)$ with the boundary DOFs $\int_{e_i} \partial_{n_i} u ds$ replaced by $\partial_{n_i} u(M_{e_i})$, where M_{e_i} is the midpoint of e_i , can be found in [11, Theorem 6.19]. The proof is based on the Bernstein-Bézier technique. The unisolvence and H^2 -conformity of the above DOFs for $k = 2, 3$ can be proved similarly. ■

Space $V_h^k(Q)$. Space $V_h^k(Q)$ is the Lagrange finite element space on \mathcal{T}_h^Q . A function $\mathbf{u} \in V_h^k(Q)$ can be determined by

- $\mathbf{u}(v)$ for all $v \in \mathcal{V}_h(Q)$;
- $\int_e \mathbf{u} \cdot \mathbf{q} ds$ for all $\mathbf{q} \in [P_{k-2}(e)]^2$ and $e \in \mathcal{E}_h(Q)$;
- $\int_Q \operatorname{div} \mathbf{u} \cdot \mathbf{q} dA$ for all $\mathbf{q} \in W_h^{k-1}(Q) \cap L_0^2(Q)$;
- $\int_Q \mathbf{u} \cdot \operatorname{curl} \mathbf{q} dA$ for all $\mathbf{q} \in \Sigma_h^{k+1}(Q) \cap H_0^2(Q)$.

Lemma 3.2. The above DOFs for $V_h^k(Q)$ are unisolvent and H^1 -conforming.

Proof. The H^1 -conformity can be easily proved by the vertex and edge DOFs. Now to show the unisolvence, we suppose that the above DOFs vanish on $\mathbf{u} \in V_h^k(Q)$ and prove that $\mathbf{u} = 0$. From integration by parts and the edge DOFs, we have

$$\int_Q \operatorname{div} \mathbf{u} dA = \int_{\partial Q} \mathbf{u} \cdot \mathbf{n}_Q ds = 0,$$

which together with the interior DOFs $\int_Q \operatorname{div} \mathbf{u} \cdot \mathbf{q} dA$ for any $\mathbf{q} \in W_h^{k-1}(Q) \cap L_0^2(Q)$ yields

$$\operatorname{div} \mathbf{u} = 0 \text{ in } Q.$$

Then for $T \in \mathcal{T}_h^Q$, there exists a function $\phi_T \in P_{k+1}(T)$ such that $\mathbf{u}|_T = \operatorname{curl} \phi_T$. Since $\mathbf{u} = 0$ on ∂Q , we have the tangential derivative of ϕ_T along $\partial T \cap \partial Q$ is 0. Without loss of generality, we can choose ϕ_T such that $\phi_T = 0$ on $\partial T \cap \partial Q$. Define a function ϕ such that $\phi|_T = \phi_T$, then $\phi = 0$ on ∂Q . Moreover, we have $\phi \in H_0^2(Q)$ since $\mathbf{u} \in \mathbf{H}_0^1(Q)$. Take $\mathbf{q} = \phi$ in the last category of DOFs for $V_h^k(Q)$, we have $\operatorname{curl} \phi = 0$ and hence $\mathbf{u} = 0$. ■

Remark 3.1. Since space $V_h^k(Q)$ is the Lagrange finite element space on \mathcal{T}_h^Q , a function $\mathbf{u} \in V_h^k(Q)$ can also be determined by

- $\mathbf{u}(v)$ for all $v \in \mathcal{V}_h(Q)$;
- $\int_e \mathbf{u} \cdot \mathbf{q} ds$, for all $\mathbf{q} \in [P_{k-2}(e)]^2$ and $e \in \mathcal{E}_h(Q)$;
- $\mathbf{u}(v_0)$ (v_0 is the intersection of the two diagonals of Q);
- $\int_{e_i^0} \mathbf{u} \cdot \mathbf{q} ds$, for all $\mathbf{q} \in [P_{k-2}(e_i^0)]^2$, $i = 1, 2, 3, 4$ (e_i^0 , $i = 1, 2, 3, 4$ are the four interior edges in Q);
- $\int_T \mathbf{u} \cdot \mathbf{q} dA$ for all $\mathbf{q} \in P_{k-3}(T)$ and $T \in \mathcal{T}_h^Q$.

Lemma 3.3. The sequence (3.2) is a complex and is exact.

Proof. From the construction, we have that the sequence is a complex. It suffices to show the exactness. The exactness at $W_h^{k-1}(Q)$ and $\Sigma_h^{k+1}(Q)$ is trivial. To show the exactness at $V_h^k(Q)$,

we suppose $\mathbf{u} \in V_h^k(Q)$ satisfying $\operatorname{div} \mathbf{u} = 0$ and show that $\mathbf{u} = \operatorname{curl} \phi$ for some ϕ in $\Sigma_h^{k+1}(Q)$. Since $V_h^k(Q)$ is a subspace of the Brezzi-Douglas-Marini finite element space, we have, from the exactness of the de Rham complex,

$$\mathbf{u} = \operatorname{curl} \phi,$$

for some ϕ in the Lagrange finite element space of order $k+1$. Due to the fact that $V_h^k(Q) \subset \mathbf{H}^1(Q)$, we can conclude that $\phi \in \Sigma_h^{k+1}(Q)$. ■

Characterization of Space $W_h^{k-1}(Q)$. To use the mixed formulation (2.1), we now give a characterization of $W_h^{k-1}(Q)$. Define

$$P_h^{k-1}(Q) = \{u \in L^2(Q) : u|_T \in P_{k-1}(T) \text{ for any } T \in \mathcal{T}_h^Q\},$$

then $W_h^{k-1}(Q)$ is a subspace of $P_h^{k-1}(Q)$.

From Lemma 3.3, we have

$$\dim W_h^{k-1}(Q) = 1 - \dim \Sigma_h^{k+1}(Q) + \dim V_h^k(Q) = \dim P_h^{k-1}(Q) - 1.$$

Therefore, to characterize $W_h^{k-1}(Q)$, we need to identify a function which is in $P_h^{k-1}(Q)$ but not in $W_h^{k-1}(Q)$.

We first characterize $W_h^{k-1}(\hat{Q})$. According to [15, Proposition 2.1], for $\hat{u} \in W_h^{k-1}(\hat{Q})$, the following condition holds

$$\hat{u}|_{\hat{T}_1}(0,0) + \hat{u}|_{\hat{T}_3}(0,0) = \hat{u}|_{\hat{T}_2}(0,0) + \hat{u}|_{\hat{T}_4}(0,0),$$

which imposes a restriction on the constant term of \hat{u} . Therefore, the piecewise constant function shown in Figure 3.3 does not belong to $W_h^{k-1}(\hat{Q})$.

Define

$$\tilde{P}_h^{k-1}(Q) = \{u \in L^2(Q) : u|_T \in \tilde{P}_{k-1}(T) \text{ for any } T \in \mathcal{T}_h^Q\}.$$

We can deduce that the space $W_h^1(\hat{Q})$ is spanned by the functions in Figure 3.4 and in $\tilde{P}_h^1(\hat{Q})$, and the space $W_h^2(\hat{Q})$ is spanned by the functions in Figure 3.4 and in $\tilde{P}_h^1(\hat{Q}) + \tilde{P}_h^2(\hat{Q})$.

We then characterize $W_h^{k-1}(Q)$ as

$$W_h^{k-1}(Q) = \{q : q = \hat{q} \circ F_Q^{-1} \text{ for } \hat{q} \in W_h^{k-1}(\hat{Q})\}.$$

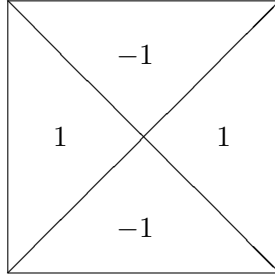
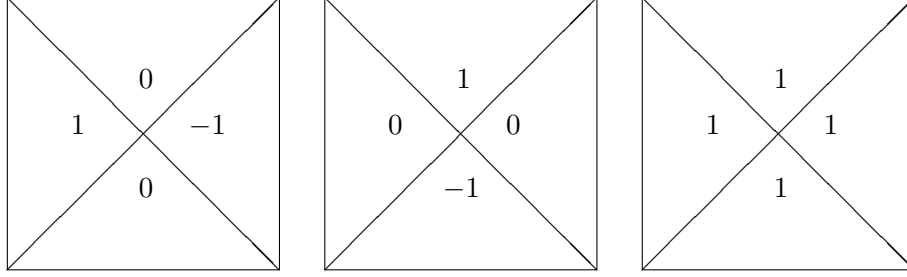


FIGURE 3.3. A piecewise constant function not in $W_h^{k-1}(\hat{Q})$

FIGURE 3.4. Piecewise constant functions in $W_h^{k-1}(\hat{Q})$.

We glue together $\Sigma_h^{k+1}(Q)$ for $Q \in \mathcal{Q}_h$ by the DOFs for $\Sigma_h^{k+1}(Q)$ to define a global finite element space Σ_h^{k+1} . Similarly, we can define V_h^k and W_h^{k-1} .

Lemma 3.4. The sequence (3.1) is an exact complex on contractible domains.

Proof. From the construction, we have the sequence is a complex. It suffices to show the exactness. The exactness at W_h^{k-1} and Σ_h^{k+1} is trivial. To show the exactness at V_h^k , we use dimension count. The dimensions of Σ_h^{k+1} and V_h^k are respectively

$$\dim \Sigma_h^{k+1} = 3\mathcal{V} + (2k-3)\mathcal{E} + 4(k-2)\mathcal{Q},$$

$$\dim V_h^k = 2\mathcal{V} + (2k-2)\mathcal{E} + \dim W_h^{k-1} - \mathcal{Q} + 4(k-2)\mathcal{Q},$$

where \mathcal{V} , \mathcal{E} , \mathcal{Q} are the number of vertices, edges and convex quadrilaterals in \mathcal{Q}_h . Then we have

$$1 - \dim \Sigma_h^{k+1} + \dim V_h^k - \dim W_h^{k-1} = 1 - \mathcal{V} + \mathcal{E} - \mathcal{Q} = 0,$$

from the Euler's formula. This completes the proof. ■

4. THE CONSTRUCTION OF FORTIN INTERPOLATION

In this section, we construct a Fortin interpolation Π_h that satisfies **H3** in Assumption 2.1. To this end, we first define an interpolation $\Pi_h^0 : V \rightarrow V_h^k$ whose restriction on Q is denoted by Π_Q^0 . For $\mathbf{u} \in V$, $\Pi_Q^0 \mathbf{u}$ is uniquely determined by

- $\Pi_Q^0 \mathbf{u}(v) = 0$ for any $v \in \mathcal{V}_h(Q)$;
- $\int_e \Pi_Q^0 \mathbf{u} \cdot \boldsymbol{\tau}_e q \, ds = 0$ for any $q \in P_{k-2}(e)$ and $e \in \mathcal{E}_h(Q)$;
- $\int_e \Pi_Q^0 \mathbf{u} \cdot \mathbf{n}_e q \, ds = \int_e \mathbf{u} \cdot \mathbf{n}_e q \, ds$ for any $q \in P_{k-2}(e)$ and $e \in \mathcal{E}_h(Q)$;
- $\int_Q \operatorname{div} \Pi_Q^0 \mathbf{u} \cdot q \, dA = \int_Q \operatorname{div} \mathbf{u} \cdot q \, dA$ for any $q \in W_h^{k-1}(Q) \cap L_0^2(Q)$;
- $\int_Q \Pi_Q^0 \mathbf{u} \cdot \operatorname{curl} q \, dA = 0$ for any $q \in \Sigma_h^k(Q) \cap H_0^2(Q)$.

Recall $P_h : L^2(\Omega) \rightarrow W_h^{k-1}$ is the L^2 -orthogonal projection. From the non-vanishing edge DOFs, we have for any $Q \in \mathcal{Q}_h$,

$$\int_Q \operatorname{div} \Pi_h^0 \mathbf{u} - P_h \operatorname{div} \mathbf{u} \, dA = \int_Q \operatorname{div} \Pi_h^0 \mathbf{u} - \operatorname{div} \mathbf{u} \, dA = \int_{\partial Q} (\Pi_h^0 \mathbf{u} - \mathbf{u}) \cdot \mathbf{n}_Q \, ds = 0,$$

which together with the non-vanishing interior DOFs leads to $\operatorname{div} \Pi_h^0 \mathbf{u} = P_h \operatorname{div} \mathbf{u}$.

We then define $\Pi_h : V \rightarrow V_h^k$ by

$$\Pi_h = \Pi_h^0(\mathbf{I} - \mathbf{I}_h) + \mathbf{I}_h, \quad (4.1)$$

where $\mathbf{I}_h : \mathbf{H}^{1/2+\delta}(\Omega) \rightarrow V_h^k$ is the Scott-Zhang interpolation defined in [14]. According to [9, Theorem 3.3], for $T \in \mathcal{T}_h$,

$$h_T^{-1/2-\delta} \|\mathbf{u} - \mathbf{I}_h \mathbf{u}\|_T + \|\mathbf{I}_h \mathbf{u}\|_{1/2+\delta, T} \leq C \|\mathbf{u}\|_{1/2+\delta, \omega(T)},$$

where $\omega(T) = \bigcup_{\substack{T' \in \mathcal{T}_h \\ \bar{T}' \cap \bar{T} \neq \emptyset}} T'$.

Under the transformation

$$\mathbf{u} \circ F_i = \frac{B_i}{|B_i|} \hat{\mathbf{u}},$$

we have

- $\int_e \mathbf{u} \cdot \mathbf{n}_e q \, ds = \int_{\hat{e}} \hat{\mathbf{u}} \cdot \hat{\mathbf{n}}_e q \, d\hat{s},$
- $\int_Q \operatorname{div} \mathbf{u} \cdot q \, dA = \int_{\hat{Q}} \widehat{\operatorname{div} \hat{\mathbf{u}}} \cdot \hat{q} \, d\hat{A},$

which implies $\widehat{\Pi_Q^0 \mathbf{u}} = \Pi_{\hat{Q}}^0 \hat{\mathbf{u}}$. By scaling argument, we obtain the following stability estimate of Π_h^0 ,

$$\begin{aligned} \|\Pi_Q^0 \mathbf{u}\|_Q^2 &\leq C \|\widehat{\Pi_Q^0 \mathbf{u}}\|_{\hat{Q}}^2 = C \|\Pi_{\hat{Q}}^0 \hat{\mathbf{u}}\|_{\hat{Q}}^2 \leq C \left(\|\hat{\mathbf{u}}\|_{1/2+\delta, \hat{Q}}^2 + \|\widehat{\operatorname{div} \hat{\mathbf{u}}}\|_{\hat{Q}}^2 \right) \\ &\leq C \left(\|\mathbf{u}\|_Q^2 + h^{1+2\delta} \|\mathbf{u}\|_{1/2+\delta, Q}^2 + h^2 \|\operatorname{div} \mathbf{u}\|_Q^2 \right). \end{aligned} \quad (4.2)$$

Theorem 4.1. The interpolation Π_h defined by (4.1) satisfies Assumption 2.1.

Proof. We first prove (2.8). For any $q_h \in W_h^{k-1}$, we have

$$\begin{aligned} (\operatorname{div} \Pi_h \mathbf{u} - P_h \operatorname{div} \mathbf{u}, q_h) &= (\operatorname{div} \Pi_h^0(\mathbf{I} - \mathbf{I}_h) \mathbf{u} + \operatorname{div} \mathbf{I}_h \mathbf{u} - P_h \operatorname{div} \mathbf{u}, q_h) \\ &= (P_h \operatorname{div}(\mathbf{I} - \mathbf{I}_h) \mathbf{u} + \operatorname{div} \mathbf{I}_h \mathbf{u} - P_h \operatorname{div} \mathbf{u}, q_h) = 0, \end{aligned}$$

which implies (2.8).

We now prove (2.9). By the definition of Π_h and the stability estimate (4.2) of Π_h^0 ,

$$\begin{aligned} \|(\mathbf{I} - \Pi_h) \mathbf{u}\|^2 &= \|(\mathbf{I} - \Pi_h^0)(\mathbf{I} - \mathbf{I}_h) \mathbf{u}\|^2 \\ &\leq C \left(\|(\mathbf{I} - \mathbf{I}_h) \mathbf{u}\|^2 + h^{1+2\delta} \|(\mathbf{I} - \mathbf{I}_h) \mathbf{u}\|_{1/2+\delta}^2 + h^2 \|\operatorname{div}(\mathbf{I} - \mathbf{I}_h) \mathbf{u}\|^2 \right). \end{aligned} \quad (4.3)$$

To estimate $\|\operatorname{div}(\mathbf{I} - \mathbf{I}_h) \mathbf{u}\|$, we introduce the canonical interpolation $\mathbf{r}_T : \mathbf{H}^{1/2+\delta}(T) \rightarrow \mathbf{P}_0(T) \oplus \mathbf{xP}_0(T)$ for $T \in \mathcal{T}_h$ such that for $\mathbf{u} \in \mathbf{H}^{1/2+\delta}(T)$,

$$\int_e \mathbf{r}_T \mathbf{u} \cdot \mathbf{n}_e \, ds = \int_e \mathbf{u} \cdot \mathbf{n}_e \, ds \quad \text{for any } e \subset \partial T.$$

Assume $\pi_T : L^2(T) \rightarrow P_0(T)$ is the L^2 -orthogonal projection. The interpolation \mathbf{r}_T satisfies [12]

$$\operatorname{div} \mathbf{r}_T \mathbf{u} = \pi_T \operatorname{div} \mathbf{u}, \quad (4.4)$$

$$\|\mathbf{u} - \mathbf{r}_h \mathbf{u}\|_T \leq C h_T^{1/2+\delta} \|\mathbf{u}\|_{1/2+\delta, T}. \quad (4.5)$$

Now we estimate $\|\operatorname{div}(\mathbf{I} - \mathbf{I}_h)\mathbf{u}\|_T$ for $T \in \mathcal{T}_h$,

$$\begin{aligned} \|\operatorname{div}(\mathbf{I} - \mathbf{I}_h)\mathbf{u}\|_T &\leq \|\operatorname{div}(\mathbf{I} - \mathbf{r}_T)\mathbf{u}\|_T + \|\operatorname{div}(\mathbf{r}_T - \mathbf{I}_h)\mathbf{u}\|_T \\ &\leq \|\operatorname{div}\mathbf{u} - \pi_T \operatorname{div}\mathbf{u}\|_T + Ch_T^{-1}\|(\mathbf{r}_T - \mathbf{I}_h)\mathbf{u}\|_T \quad ((4.4) \text{ and inverse inequality}) \\ &\leq C\|\operatorname{div}\mathbf{u}\|_T + Ch_T^{-1}\|\mathbf{r}_T\mathbf{u} - \mathbf{u}\|_T + Ch_T^{-1}\|\mathbf{u} - \mathbf{I}_h\mathbf{u}\|_T \\ &\leq C\|\operatorname{div}\mathbf{u}\|_T + Ch_T^{-1/2+\delta}\|\mathbf{u}\|_{1/2+\delta,T} + Ch_T^{-1}\|\mathbf{u} - \mathbf{I}_h\mathbf{u}\|_T, \end{aligned}$$

which, plugged into (4.3), leads to

$$\begin{aligned} \|(\mathbf{I} - \Pi_h)\mathbf{u}\|^2 &\leq C \left(\|(\mathbf{I} - \mathbf{I}_h)\mathbf{u}\|^2 + h^{1+2\delta}\|(\mathbf{I} - \mathbf{I}_h)\mathbf{u}\|_{1/2+\delta}^2 + h^2\|\operatorname{div}\mathbf{u}\|^2 + Ch^{1+2\delta}\|\mathbf{u}\|_{1/2+\delta}^2 \right) \\ &\leq C \left(h^{1+2\delta}\|\mathbf{u}\|_{1/2+\delta}^2 + h^2\|\operatorname{div}\mathbf{u}\|^2 \right) \leq Ch^{1+2\delta}\|\mathbf{u}\|_V^2. \end{aligned}$$

■

Theorem 4.2. In addition to Assumption 2.1, the interpolation Π_h defined by (4.1) also satisfies

$$\|\Pi_h\mathbf{u}\|_1 \leq C\|\mathbf{u}\|_1.$$

Then Π_h defines a V -bounded cochain projection for the complex (1.4).

Proof. By Theorem 4.1, we have

$$\|\Pi_h\mathbf{u}\| \leq C\|\mathbf{u}\|_1.$$

It remains to show that

$$\|\operatorname{grad}\Pi_h\mathbf{u}\| \leq C\|\mathbf{u}\|_1.$$

According to the definition of Π_h , the inverse inequality, (4.2), and the approximation property \mathbf{I}_h , we have

$$\begin{aligned} \|\operatorname{grad}\Pi_h\mathbf{u}\|^2 &= \|\operatorname{grad}\Pi_h^0(\mathbf{u} - \mathbf{I}_h\mathbf{u}) + \operatorname{grad}\mathbf{I}_h\mathbf{u}\|^2 \\ &\leq Ch^{-2}\|\Pi_h^0(\mathbf{u} - \mathbf{I}_h\mathbf{u})\|^2 + \|\operatorname{grad}\mathbf{I}_h\mathbf{u}\|^2 \\ &\leq C(\|\mathbf{u} - \mathbf{I}_h\mathbf{u}\|^2 + h^2\|\mathbf{u} - \mathbf{I}_h\mathbf{u}\|_1^2 + h^2\|\operatorname{div}(\mathbf{u} - \mathbf{I}_h\mathbf{u})\|^2 + \|\mathbf{I}_h\mathbf{u}\|_1^2) \\ &\leq C(\|\mathbf{u} - \mathbf{I}_h\mathbf{u}\|^2 + h^2\|\mathbf{u}\|_1^2 + \|\mathbf{I}_h\mathbf{u}\|_1^2) \leq C\|\mathbf{u}\|_1^2. \end{aligned}$$

■

5. BOUNDED COMMUTING PROJECTIONS

In this section, we will construct bounded commuting projections for the complexes (1.4). To be specific, we will construct π_h by mimicking the Scott-Zhang interpolation [10, 14] and $\tilde{\Pi}_h$ by modifying Π_h in Section 4 such that the following diagram commutes:

$$\begin{array}{ccccccccc} 0 & \longrightarrow & \mathbb{R} & \xrightarrow{\subset} & H^2(\Omega) & \xrightarrow{\operatorname{curl}} & \mathbf{H}^1(\Omega) & \xrightarrow{\operatorname{div}} & L^2(\Omega) & \longrightarrow & 0 \\ & & \downarrow \mathbf{I} & & \downarrow \pi_h & & \downarrow \tilde{\Pi}_h & & \downarrow P_h & & \\ 0 & \longrightarrow & \mathbb{R} & \xrightarrow{\subset} & \Sigma_h^{k+1} & \xrightarrow{\operatorname{curl}} & V_h^k & \xrightarrow{\operatorname{div}} & \operatorname{div} V_h^k & \longrightarrow & 0. \end{array} \quad (5.1)$$

The construction of π_h . We denote by $\mathcal{N}_h = \mathcal{N}_h^0 \cup \mathcal{N}_h^1$ the set of DOFs for Σ_h^{k+1} with $\mathcal{N}_h^0 = \{N_i, i = 1, 2, \dots, 2\mathcal{V} : N_i u = D_j u(v) \text{ for some } j \in \{1, 2\}, v \in \mathcal{V}_h \text{ with } D_1 = \partial_x, D_2 = \partial_y\}$, and

$$\mathcal{N}_h^1 = \{N_i, i = 2\mathcal{V} + 1, \dots, \dim \mathcal{N}_h : N_i \text{ is the DOF in } \mathcal{N}_h \text{ but not in } \mathcal{N}_h^0\}.$$

For $u \in H^{2+\delta}(\Omega)$, we can define a canonical interpolation $\tilde{\pi}_h : H^{2+\delta}(\Omega) \rightarrow \Sigma_h^{k+1}$ by the DOFs in \mathcal{N}_h :

$$\tilde{\pi}_h u = \sum_{i=1}^{2\mathcal{V}} N_i(u) \phi_i + \sum_{i=2\mathcal{V}+1}^{\dim \mathcal{N}_h} N_i(u) \phi_i = \sum_{v \in \mathcal{V}_h} \sum_{j=1}^2 D_j u(v) \phi_j^v + \sum_{i=2\mathcal{V}+1}^{\dim \mathcal{N}_h} N_i(u) \phi_i,$$

where $\{\phi_i\}_{i=1}^{\dim \mathcal{N}_h}$ is the nodal basis of Σ_h^{k+1} such that $N_i(\phi_j) = \delta_{ij}$ for $N_i \in \mathcal{N}_h$. For $i = 1, 2, \dots, 2\mathcal{V}$, there exists j and v such that $\phi_i = \phi_j^v$.

By scaling argument,

$$\|\phi_j^v\|_{m,Q} \leq Ch_Q^{2-m}, \quad j = 1, 2, \quad v \in \mathcal{V}_h, \quad \|\phi_i\|_{m,Q} \leq Ch_Q^{1-m}, \quad \text{for } i = 2\mathcal{V} + 1, \dots, \dim \mathcal{N}_h. \quad (5.2)$$

The DOFs in \mathcal{N}_h^0 are not well defined for $u \in H^2(\Omega)$. To define the mapping $\pi_h : H^2(\Omega) \rightarrow \Sigma_h^{k+1}$, we modify DOFs in \mathcal{N}_h^0 by adopting a similar approach to the one outlined in [10, (4.11)]. However, we deviate by setting the parameter b_κ in their equation (4.11) to 1. For $v \in \mathcal{V}_h$, we select any edge e_v such that

$$v \in \overline{e_v},$$

subject to the restriction $e_v \in \partial\Omega$ if $v \in \partial\Omega$.

For $v \in \mathcal{V}_h$, according to Riesz's Representation Theorem, there exists a unique function $\psi_v \in P_{k+1}(e_v)$ such that

$$\int_{e_v} \psi_v(\mathbf{x}) w(\mathbf{x}) d\mathbf{x} = w(v) \text{ for any } w \in P_{k+1}(e_v).$$

Note that ψ_v depends on the choice of e_v . By construction, we have

$$\int_{e_v} \psi_v(\mathbf{x}) D_j \phi_i(\mathbf{x}) d\mathbf{x} = 0 \text{ for } i = 2\mathcal{V} + 1, \dots, \dim \mathcal{N}_h \text{ and } j = 1, 2, \quad (5.3)$$

$$\int_{e_v} \psi_v(\mathbf{x}) D_j \phi_{j'}^{v'}(\mathbf{x}) d\mathbf{x} = \delta_{(j,v),(j',v')}. \quad (5.4)$$

Then we define

$$\pi_h u = \sum_{v \in \mathcal{V}_h} \sum_{j=1,2} \int_{e_v} \psi_v(\mathbf{x}) D_j u(\mathbf{x}) d\mathbf{x} \phi_j^v + \sum_{i=2\mathcal{V}+1}^{\dim \mathcal{N}_h} N_i(u) \phi_i.$$

By (5.3)–(5.4), we conclude that π_h is a projection,

$$\pi_h u = u \quad \text{for any } u \in \Sigma_h.$$

According to [10, (4.12)],

$$\|\psi_v\|_{L^\infty(e_v)} \leq Ch^{-1}.$$

It follows from [14, (3.6)] that

$$\|\operatorname{grad} u\|_{L^1(e_v)} \leq C \sum_{\ell=1}^2 h_{T_v}^{\ell-1} |u|_{\ell, T_v} \quad \forall u \in H^2(T_v), \quad (5.5)$$

where T_v is a triangle in \mathcal{T}_h that contains e_v as an edge.

Theorem 5.1. Let $u \in H^2(\Omega)$. Then

$$\|\pi_h u\|_{m, Q} \leq C \sum_{\ell=0}^2 h^{\ell-m} |u|_{\ell, S_Q}, \quad m = 0, 1, 2,$$

where

$$S_Q = \operatorname{interior}(\cup \{\bar{T} \in \mathcal{T}_h : \bar{T} \cap \bar{Q} \neq \emptyset\}).$$

Proof. We denote by $\mathcal{N}_h(Q) = \mathcal{N}_h^0(Q) \cup \mathcal{N}_h^1(Q)$ the set of DOFs for $V_h^k(Q)$. Then for $N_i \in \mathcal{N}_h^1(Q)$, by (5.5) and the embedding theorem, we have

$$\begin{aligned} |N_i(u)| &\leq C \sum_{e \in \mathcal{E}_h(Q)} \|\operatorname{grad} u\|_{L^1(e)} + C \|u\|_{L^\infty(Q)} \leq C \sum_{\ell=1}^2 h^{\ell-1} |u|_{\ell, S_Q} + \|\hat{u}\|_{L^\infty(\hat{Q})} \\ &\leq C \sum_{\ell=1}^2 h^{\ell-1} |u|_{\ell, S_Q} + \|\hat{u}\|_{H^2(\hat{Q})} \leq C \sum_{\ell=0}^2 h^{\ell-1} |u|_{\ell, S_Q}, \end{aligned}$$

where C is independent on h^{-1} .

$$\begin{aligned} \|\pi_h u\|_{m, Q} &\leq \sum_{N_i \in \mathcal{N}_h(Q)} |N_i(\pi_h u)| \|\phi_i\|_{m, Q} \\ &\leq C h^{2-m} \sum_{N_i \in \mathcal{N}_h^0(Q)} |N_i(\pi_h u)| \|\hat{\phi}_i\|_{m, \hat{Q}} + C h^{1-m} \sum_{N_i \in \mathcal{N}_h^1(Q)} |N_i(\pi_h u)| \|\hat{\phi}_i\|_{m, \hat{Q}} \\ &\leq C h^{2-m} \sum_{v \in \mathcal{V}_h(K)} \sum_{j=1,2} \left| \int_{e_v} \psi_v(\mathbf{x}) D_j u(\mathbf{x}) d\mathbf{x} \right| + \sum_{N_i \in \mathcal{N}_h^1(Q)} C h^{1-m} |N_i(u)| \\ &\leq C h^{2-m} \sum_{v \in \mathcal{V}_h(K)} \sum_{j=1,2} \|\psi_v\|_{L^\infty(e_v)} \|D_j u\|_{L^1(e_v)} + \sum_{N_i \in \mathcal{N}_h^1(Q)} C h^{1-m} |N_i(u)| \\ &\leq C h^{\ell-m} \sum_{v \in \mathcal{V}_h(K)} \sum_{\ell=1}^2 |u|_{\ell, T_v} + C h^{\ell-m} \sum_{\ell=0}^2 |u|_{\ell, S_Q} \leq C h^{\ell-m} \sum_{\ell=0}^2 |u|_{\ell, S_Q}. \end{aligned}$$

■

Theorem 5.2. Let $u \in H^2(\Omega)$. Then

$$\sum_{Q \in \mathcal{Q}_h} h_Q^{2(m-l)} \|u - \pi_h u\|_{m, Q}^2 \leq C |u|_l^2,$$

with integer $0 \leq m \leq l \leq 2$.

Proof. By following the argument used in [14, Theorem 4.1] and using Theorem 5.1, we can prove the theorem. ■

The construction of $\tilde{\Pi}_h$. An H^1 -orthogonal decomposition for $\mathbf{u} \in \mathbf{H}^1(\Omega)$ leads to

$$\mathbf{u} = \text{grad } w + \mathbf{u}^\perp,$$

where $w \in H^2(\Omega)$ with $\int_\Omega w = 0$ and $\mathbf{u}^\perp \in \{\mathbf{H}^1(\Omega) : (\mathbf{u}^\perp, \mathbf{q}) + (\text{grad } \mathbf{u}^\perp, \text{grad } \mathbf{q}) = 0 \text{ for any } \mathbf{q} \in \text{grad } H^2(\Omega)\}$. Then

$$\|\text{grad } w\|_1 + \|\mathbf{u}^\perp\|_1 \leq \|\mathbf{u}\|_1.$$

We define $\tilde{\Pi}_h : \mathbf{H}^1(\Omega) \rightarrow V_h^k$ by

$$\tilde{\Pi}_h \mathbf{u} = \text{grad } \pi_h w + \Pi_h \mathbf{u}^\perp.$$

Clearly, we have the commutative property,

$$\tilde{\Pi}_h \text{grad } w = \text{grad } \pi_h w, \quad \text{curl } \tilde{\Pi}_h \mathbf{u} = P_h \text{curl } \mathbf{u}. \quad (5.6)$$

Theorem 5.3. Let $\mathbf{u} \in \mathbf{H}^1(\Omega)$. Then

$$\|\mathbf{u} - \tilde{\Pi}_h \mathbf{u}\| \leq Ch \|\mathbf{u}\|_1, \quad (5.7)$$

$$\|\tilde{\Pi}_h \mathbf{u}\|_1 \leq C \|\mathbf{u}\|_1. \quad (5.8)$$

Proof. By the triangle inequality, Theorem 5.2, Theorem 4.1, and the Poincaré inequality,

$$\begin{aligned} \|\mathbf{u} - \tilde{\Pi}_h \mathbf{u}\| &\leq \|\text{grad } w - \text{grad } \pi_h w\| + \|\mathbf{u}^\perp - \Pi_h \mathbf{u}^\perp\| \\ &\leq Ch \|w\|_2 + Ch \|\mathbf{u}^\perp\|_1 \leq Ch \|\text{grad } w\|_1 + Ch \|\mathbf{u}^\perp\|_1 \leq Ch \|\mathbf{u}\|_1. \end{aligned}$$

Similarly, by Theorem 4.2, we can prove (5.8). ■

Theorem 5.4. Define the cohomology space for the top complex in (1.4)

$$\begin{aligned} \mathcal{H}^0 &:= \ker (\text{curl} : H^2(\Omega) \rightarrow \mathbf{H}^1(\Omega)) / \mathbb{R}, \quad \mathcal{H}^2 := \text{ran} (\text{div} : \mathbf{H}^1(\Omega) \rightarrow L^2(\Omega)), \\ \mathcal{H}^1 &:= \ker (\text{div} : \mathbf{H}^1(\Omega) \rightarrow L^2(\Omega)) / \text{ran} (\text{curl} : H^2(\Omega) \rightarrow \mathbf{H}^1(\Omega)), \end{aligned}$$

and the cohomology spaces for the bottom complex in (1.4)

$$\begin{aligned} \mathcal{H}_h^0 &:= \ker (\text{curl} : \Sigma_h \rightarrow V_h) / \mathbb{R}, \quad \mathcal{H}_h^2 := \text{ran} (\text{div} : V_h \rightarrow \text{div } V_h), \\ \mathcal{H}_h^1 &:= \ker (\text{div} : V_h \rightarrow \text{div } V_h) / \text{ran} (\text{curl} : \Sigma_h \rightarrow V_h). \end{aligned}$$

Then the interpolations π_h , $\tilde{\Pi}_h$, and P_h induce an isomorphism from \mathcal{H}^ℓ onto \mathcal{H}_h^ℓ .

Proof. By (5.6) and Theorems 5.2 and 5.8, the interpolations π_h , $\tilde{\Pi}_h$, and P_h are bounded commuting projections. Then to prove the theorem, according to Theorem 5.1 in [2], it suffices to show [2, (5.8)]. We only show [2, (5.8)] for Π_h . It reads

$$\|\varphi - \Pi_h \varphi\| < \|\varphi\|, \quad 0 \neq \varphi \in \mathfrak{H}^1,$$

where \mathfrak{H}^1 is the space of harmonic 1-forms with dimension equal to the first Betti number of the domain Ω . From Theorem 4.1,

$$\|\varphi - \Pi_h \varphi\| \leq Ch \|\varphi\|_1 \leq Ch \|\varphi\| < \|\varphi\|, \text{ for } h \text{ small enough,}$$

where we have used the norm equivalence for the finite-dimensional space \mathfrak{H}^1 . ■

6. NUMERICAL EXAMPLES

6.1. Example 1. In this example, we compute eigenvalues of (2.1) on a square domain $\Omega = (0, \pi) \times (0, \pi)$ using quadratic and cubic Lagrange elements on criss-cross mesh. Figure 6.1 shows two criss-cross meshes of Ω with $h = \pi/8$: a rectangular criss-cross mesh and a quadrilateral criss-cross mesh.

In Tables 6.1 and 6.3, we present the first ten eigenvalues and errors computed by quadratic Lagrange elements on rectangular and quadrilateral criss-cross meshes for a fixed $h = \pi/64$. In Tables 6.2 and 6.4, we list the rates of convergence of the first eigenvalue.

In Table 6.5, we show the first ten eigenvalues and errors computed by cubic Lagrange elements on a rectangular Criss-cross mesh for a fixed $h = \pi/64$. In Table 6.6, we list the rate of convergence of the first eigenvalue.

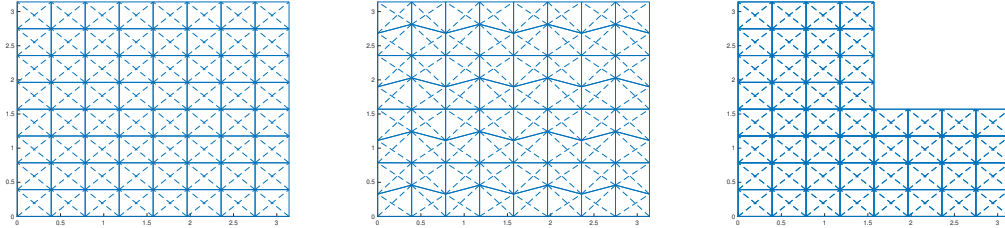


FIGURE 6.1. A rectangular criss-cross mesh of $(0, \pi) \times (0, \pi)$ (left), a quadrilateral criss-cross mesh of $(0, \pi) \times (0, \pi)$ (middle), and a rectangular criss-cross mesh of $(0, \pi) \times (0, \pi) \setminus [\frac{\pi}{2}, \pi) \times [\frac{\pi}{2}, \pi)$ (right) with $h = \pi/8$

6.2. Example 2. In this example, we compute eigenvalues of discrete problem (2.1) on an L-shape domain $\Omega = (0, \pi) \times (0, \pi) \setminus [\frac{\pi}{2}, \pi) \times [\frac{\pi}{2}, \pi)$ using quadratic Lagrange elements on a criss-cross mesh. Figure 6.1 shows a rectangular criss-cross mesh of Ω with $h = \pi/8$.

In the third column of Table 6.7, we show the first ten eigenvalues computed by quadratic Lagrange elements on the rectangular criss-cross mesh for a fixed $h = \pi/64$. In the second column, we list the first ten eigenvalues computed by the primal formulation (2.2) with quadratic Lagrange elements on the same mesh. We can see from the table that the quadratic Lagrange elements on criss-cross meshes can produce correctly convergent eigenvalues for (1.2) on the L-shape domain.

TABLE 6.1. Example 1: first ten numerical eigenvalues with $k = 2$ and $h = \pi/64$ on rectangular criss-cross mesh

i	$\lambda^{(i)}$	$\lambda_h^{(i)}$	$ \lambda^{(i)} - \lambda_h^{(i)} $
1	2	2.000000009674456	9.674455903052603e-09
2	5	5.000000169214253	1.692142532760954e-07
3	5	5.000000169215196	1.692151956333987e-07
4	8	8.000000618708425	6.187084249376085e-07
5	10	10.00000146560498	1.465604976047530e-06
6	10	10.00000146561097	1.465610974804576e-06
7	13	13.00000278345120	2.783451204636020e-06
8	13	13.00000278345120	2.783451204636020e-06
9	17	17.00000746915364	7.469153640471404e-06
10	17	17.00000746915827	7.469158269657328e-06

TABLE 6.2. Example 1: convergence rate of the first eigenvalue $k = 2$ on rectangular criss-cross mesh

h	$ \lambda^{(1)} - \lambda_h^{(1)} $	rate
$\pi/8$	3.918771488331529e-05	-
$\pi/16$	2.468843263603304e-06	3.9885
$\pi/32$	1.546846171152083e-07	3.9964
$\pi/64$	9.674455903052603e-09	3.9990

TABLE 6.3. Example 1: first ten numerical eigenvalues with $k = 2$ and $h \approx \pi/64$ on quadrilateral criss-cross mesh

i	$\lambda^{(i)}$	$\lambda_h^{(i)}$	$ \lambda^{(i)} - \lambda_h^{(i)} $
1	2	2.000000013083459	1.308345876083195e-08
2	5	5.000000196097877	1.960978774917521e-07
3	5	5.000000242443800	2.424438001469298e-07
4	8	8.000000836667605	8.366676045312715e-07
5	10	10.000001598937962	1.598937961588831e-06
6	10	10.000002092860292	2.092860292179921e-06
7	13	13.000003434403844	3.434403843982636e-06
8	13	13.000003955633003	3.955633003371872e-06
9	17	17.000007950604662	7.950604661743910e-06
10	17	17.000010623894767	1.062389476658154e-05

ACKNOWLEDGEMENT

The work of KH was supported by a Royal Society University Research Fellowship (URF\R1\221398).

TABLE 6.4. Example 1: convergence rate of the first eigenvalue $k = 2$ on quadrilateral criss-cross mesh

h	$ \lambda^{(1)} - \lambda_h^{(1)} $	rate
$\pi/8$	5.287702674161565e-05	-
$\pi/16$	3.337272737269359e-06	3.9859
$\pi/32$	2.091739674803250e-07	3.9959
$\pi/64$	1.308399699695428e-08	3.9988

TABLE 6.5. Example 1: first ten numerical eigenvalues with $k = 3$ and $h = \pi/64$ on rectangular criss-cross mesh

i	$\lambda^{(i)}$	$\lambda_h^{(i)}$	$ \lambda^{(i)} - \lambda_h^{(i)} $
1	2	2.000000009674193	9.674193002240372e-09
2	5	5.000000169214921	1.692149211862670e-07
3	5	5.000000169214921	1.692149211862670e-07
4	8	8.000000618707245	6.187072454366671e-07
5	10	10.000001465604944	1.465604944073107e-06
6	10	10.000001465605909	1.465605908634871e-06
7	13	13.000002783449016	2.783449016163786e-06
8	13	13.000002783451830	2.783451829913020e-06
9	17	17.000007469156596	7.469156596329185e-06
10	17	17.000007469156596	7.469156596329185e-06

TABLE 6.6. Example 1: convergence rate of the first eigenvalue $k = 3$ on rectangular criss-cross mesh

h	$ \lambda^{(1)} - \lambda_h^{(1)} $	rate
$\pi/8$	3.918771494682005e-05	-
$\pi/16$	2.468843251612896e-06	3.9885
$\pi/32$	1.546833066079500e-07	3.9964
$\pi/64$	9.674193002240372e-09	3.9990

REFERENCES

- [1] A Alonso-Rodríguez, Jessika Camaño, Rodolfo Rodríguez, Alberto Valli, and Pablo Venegas. Finite element approximation of the spectrum of the curl operator in a multiply connected domain. *Foundations of Computational Mathematics*, 18(6):1493–1533, 2018.
- [2] D. N. Arnold. *Finite element exterior calculus*. SIAM, 2018.
- [3] D. N. Arnold and J. Qin. Quadratic velocity/linear pressure Stokes elements. *Advances in computer methods for partial differential equations*, 7:28–34, 1992.
- [4] Douglas N Arnold, Richard S Falk, and Ragnar Winther. Finite element exterior calculus, homological techniques, and applications. *Acta numerica*, 15:1–155, 2006.
- [5] D. Boffi. Finite element approximation of eigenvalue problems. *Acta numerica*, 19:1–120, 2010.

TABLE 6.7. Example 2: first ten numerical eigenvalues with $k = 2$ and $h = \pi/80$ on rectangular mesh

i	$\lambda_{\text{primal}}^{(i)}$	$\lambda_h^{(i)}$
1	3.907542086020698	3.905354563577878
2	6.159216512440113	6.159213093492622
3	8.000000359186648	8.000000253513941
4	11.964607939274400	11.964606066013996
5	12.935434918397130	12.930090853126162
6	16.810290508710921	16.806272631957246
7	18.216953452465365	18.216933140031713
8	20.000007388434128	20.000004430751620
9	20.000007388434170	20.000004430753396
10	22.984997819905693	22.980510520283705

- [6] D. Boffi, F. Brezzi, and L. Gastaldi. On the problem of spurious eigenvalues in the approximation of linear elliptic problems in mixed form. *Mathematics of computation*, 69(229):121–140, 2000.
- [7] D. Boffi, P. Fernandes, L. Gastaldi, and I. Perugia. Computational models of electromagnetic resonators: analysis of edge element approximation. *SIAM journal on numerical analysis*, 36(4):1264–1290, 1999.
- [8] D. Boffi, J. Guzmán, and M. Neilan. Convergence of lagrange finite elements for the maxwell eigenvalue problem in two dimensions. *IMA Journal of Numerical Analysis*, 02 2022. drab104.
- [9] P. Ciarlet. Analysis of the Scott-Zhang interpolation in the fractional order Sobolev spaces. *Journal of Numerical Mathematics*, 21(3):173–180, 2013.
- [10] V. Girault and L. Scott. Hermite interpolation of nonsmooth functions preserving boundary conditions. *Mathematics of Computation*, 71(239):1043–1074, 2002.
- [11] M.-J. Lai and L. L. Schumaker. *Spline functions on triangulations*. Number 110. Cambridge University Press, 2007.
- [12] P. Monk. *Finite Element Methods for Maxwell's Equations*. Oxford University Press, 2003.
- [13] Ana Alonso Rodriguez, Enrico Bertolazzi, Riccardo Ghiloni, and Alberto Valli. Construction of a finite element basis of the first de rham cohomology group and numerical solution of 3d magnetostatic problems. *SIAM Journal on Numerical Analysis*, 51(4):2380–2402, 2013.
- [14] L. R. Scott and S. Zhang. Finite element interpolation of nonsmooth functions satisfying boundary conditions. *Mathematics of computation*, 54(190):483–493, 1990.
- [15] L Ridgway Scott and Michael Vogelius. Norm estimates for a maximal right inverse of the divergence operator in spaces of piecewise polynomials. *ESAIM: Mathematical Modelling and Numerical Analysis*, 19(1):111–143, 1985.

SCHOOL OF MATHEMATICS, THE UNIVERSITY OF EDINBURGH, JAMES CLERK MAXWELL BUILDING, PETER GUTHRIE TAIT RD, EDINBURGH EH9 3FD, UK.

Email address: `kaibo.hu@ed.ac.uk`

DEPARTMENT OF MATHEMATICAL SCIENCES, MICHIGAN TECHNOLOGICAL UNIVERSITY, HOUGHTON, MI 49931, USA.

Email address: `jiguangs@mtu.edu`

DEPARTMENT OF MATHEMATICAL SCIENCES, MICHIGAN TECHNOLOGICAL UNIVERSITY, HOUGHTON, MI 49931, USA.

Email address: `qzhang15@mtu.edu`